Supporting Information

$Co_3O_4/NiCo_2O_4$ Perforated Nanosheets for High-Energy-Density All-Solid-State Asymmetric Supercapacitors with Extended Cyclic Stability

Mahesh Kumar Paliwal and Sumanta Kumar Meher*

Department of Chemistry, Malaviya National Institute of Technology Jaipur, Rajasthan 302017, India

Email*: skmeher.chy@mnit.ac.in

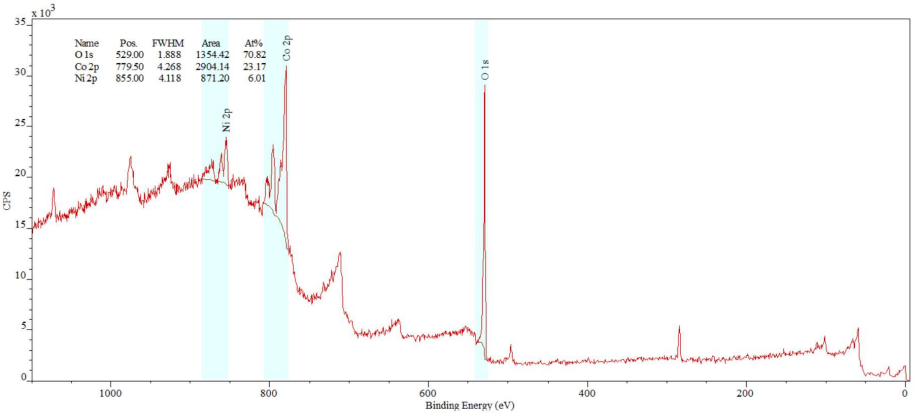

Figure S1. The survey spectrum of $Co_3O_4/NiCo_2O_4$ showing the atomic percentage of different elements.

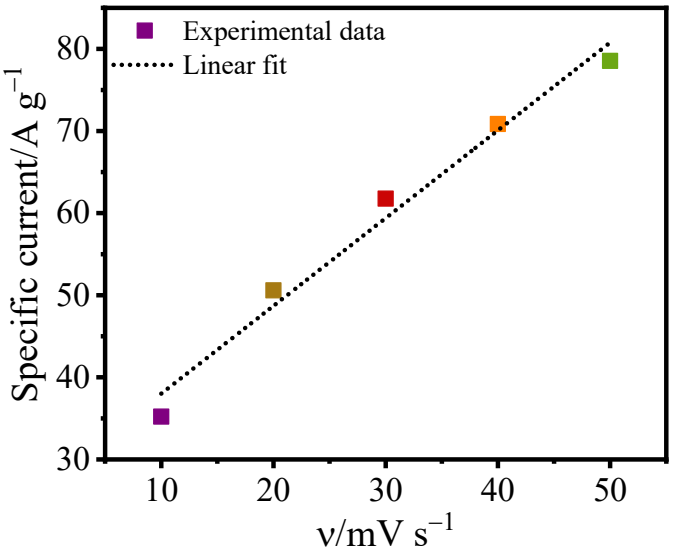

Figure S2. The linear fitted plot of anodic peak current density vs sweep rate for $Co_3O_4/NiCo_2O_4$ perforated nanosheets.

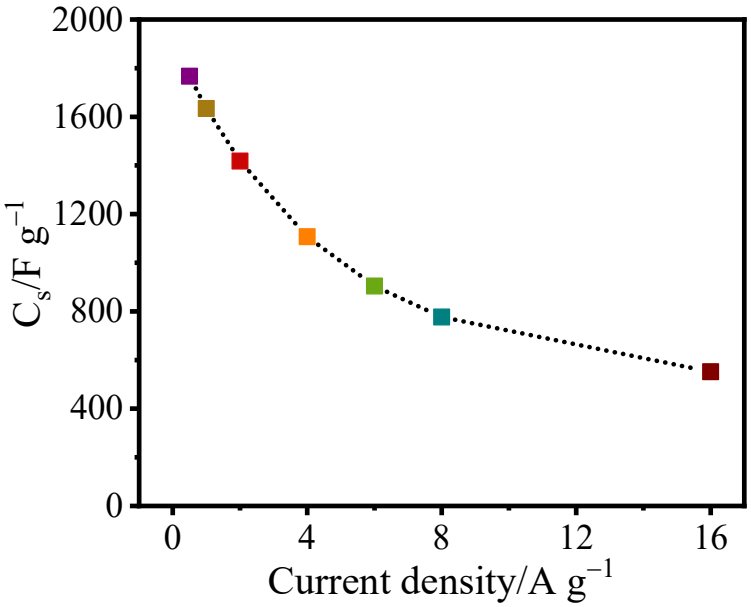

Figure S3. The plot of specific capacitance vs applied current density of $Co_3O_4/NiCo_2O_4$ perforated nanosheets.

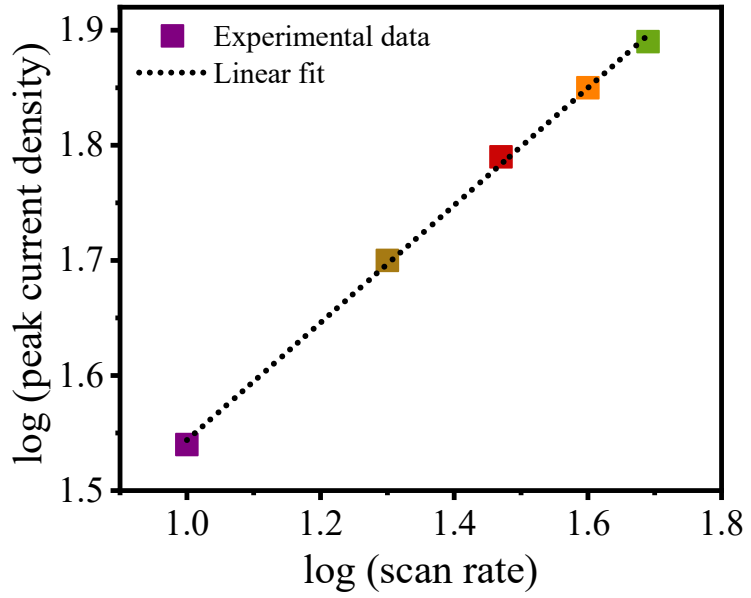

Figure S4. The plot of anodic peak current density at various potential sweep rates of $Co_3O_4/NiCo_2O_4$ perforated nanosheets.

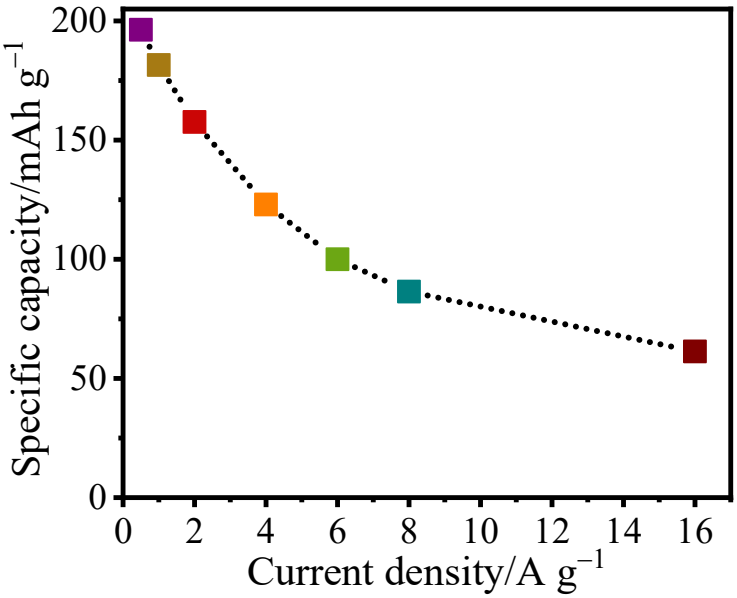

Figure S5. Specific capacity values of $Co_3O_4/NiCo_2O_4$ perforated nanosheets plotted against different applied current densities.

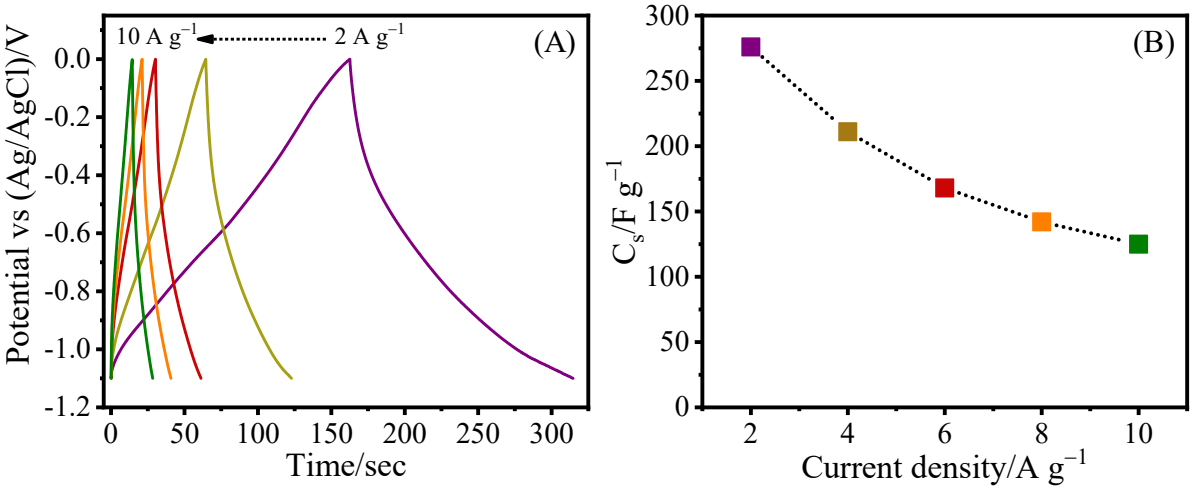

Figure S6. (A) shows the GCD profiles of N-rGO at various applied current densities of 2, 4, 6, 8 and 10 A g^{-1}; and (B) shows the corresponding C_s vs applied current density plot.

The GCD analyses of N-rGO was performed at various applied current densities of 2, 4, 6, 8, and 10 A g^{-1} within a potential window of –1.1 to 0 V, and the corresponding GCD profiles are presented in Figure S6A. The mass-specific (C_s) capacitance values of N-rGO are derived using the expression: $C_s = \frac{i \times \Delta t}{m \times \Delta V}$, where *i*, *Δt*, *m*, and *ΔV* are the applied discharge current density (A g^{-1}), discharge time (s), mass of the active electrode material (g) and the applied

potential window (V), respectively. The calculated mass-specific capacitance values are plotted against the applied current density and presented in Figure 6SB. The N-rGO demonstrates specific capacitance value of 276, 211, 168, 142, and 125 F g^{-1} at applied current densities of 2, 4, 6, 8, and 10 A g^{-1}, respectively. Additionally, the rate capacitance of N-rGO at a maximum current density of 10 A g^{-1} is found to be ~45.45%. The good electrochemical performance of N-rGO is attributed to (i) N doping, which increases the electronic conductivity by generating surface defects and free charge-carrier and (ii) the residual oxygenic functional groups on the surface of N-rGO, which increase the wettability and offer unimpeded diffusion of electrolyte ions, even at high rate conditions.[s1-s5]

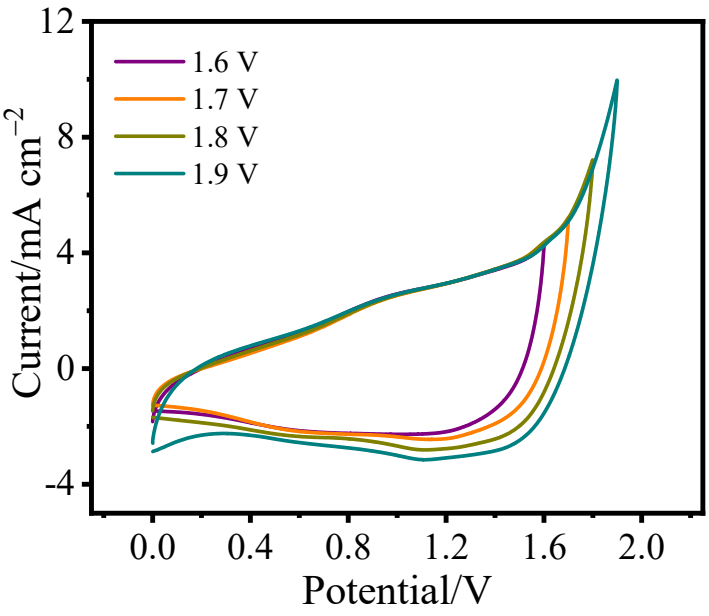

Figure S7. CV profiles of $Co_3O_4/NiCo_2O_4$||N-rGO ASSASC device in different voltage window, at an applied scan rate of 10 mV s^{-1}.

Table S1. The comparison of the capacitance and cyclic stability data of $Co_3O_4/NiCo_2O_4$||N-rGO ASSASC device with other Co_3O_4 and $NiCo_2O_4$ based asymmetric supercapacitor devices.

Sl. No.	ASC device	Capacitance	Cyclic stability	Reference
1.	α-$Co(OH)_2/Co_3O_4$||Activated Carbon	62 (F g^{-1}) at 0.5 A g^{-1}	104% at 1 A g^{-1} (2000 cycles)	[s6]
2.	Co_3O_4@MnO_2||Microwave exfoliated graphite oxide activated graphene	49.8 (F g^{-1}) at 1 A g^{-1}	81.1% at 3 A g^{-1} (10000 cycles)	[s7]
3.	$NaCoPO_4$–Co_3O_4||Graphene	28.6 (mF cm^{-2}) at 0.1 mA cm^{-2}	94.5% at 1 mA cm^{-2} (5000 cycles)	[s8]
4.	$NiCo_2O_4$/Carbon cloth||3D Porous graphene paper	71.32 (F g^{-1}) at 5 mA cm^{-2}	96.8% at 100 mA cm^{-2} (5000 cycles)	[s9]
5.	$NiCo_2O_4$/NiO||Fe_2O_3	79 (F g^{-1}) at 1 mA cm^{-2}	97% at 5 mA cm^{-2} (5000 cycles)	[s10]
6.	Ni wire/Co_3O_4@MnO_2||Carbon fibers/Graphene	13.9 (mF cm^{-2}) at 0.1 mA cm^{-2}	82% at 0.6 mA cm^{-2} (1000 cycles)	[s11]
7.	$Co_3O_4/Co(OH)_2$||Activated carbon	210 (mF cm^{-2}) at 0.3 mA cm^{-2}	97.4% at 0.5 mA cm^{-2} (5000 cycles)	[s12]
8.	$NiCo_2O_4$||Activated carbon	68.7 (F g^{-1}) at 1 A g^{-1}	87.8% at 5 A g^{-1} (2000 cycles)	[s13]
9.	$NiCo_2O_4$@Ni wire||Fe_3O_4@Ni wire	81.6 (F g^{-1}) at 1 A g^{-1}	94.8% at 5 A g^{-1} (20000 cycles)	[s14]
10.	$MoS_2/NiCo_2O_4$||Activated carbon	51.7 (F g^{-1}) at 1.5 A g^{-1}	98.2% at 6 A g^{-1} (8000 cycles)	[s15]
11.	$Co_3S_4/NiCo_2O_4$||Activated carbon	39 (F g^{-1}) at 1 A g^{-1}	84.7% (3000 cycles)	[s16]
12.	Co_3O_4@NiO||Activated carbon	134 (mF cm^{-2}) at 2 mA cm^{-2}	73.5% at 10 mA cm^{-2} (10000 cycles)	[s17]
13.	Co_3O_4/Carbon nanotubes||Fe_3O_4/Carbon nanotubes	80 (F g^{-1}) at 1 A g^{-1}	87% at 5 A g^{-1} (5000 cycles)	[s18]
14.	$NiCo_2O_4$||Activated carbon	69 (F g^{-1}) at 1 A g^{-1}	90% at 0.25 A g^{-1} (2000 cycles)	[s19]
15.	$Co_3O_4/NiCo_2O_4$||N-doped reduced graphene oxide	83 (F g^{-1}) and 251 (mF cm^{-2}) at 5 mA cm^{-2}	93.8% at 12 mA cm^{-2} (10000 cycles)	**This work**

Table S2. The comparison of cyclic stability of $Co_3O_4/NiCo_2O_4$||N-rGO ASSASC device with other asymmetric supercapacitor devices based on N-rGO or its composite as the negative electrode material.

Sl. No.	Positive electrode Material	Negative electrode Material	Cyclic stability of the ASC device	Reference
1.	α-MnS/N-rGO	N-rGO	81.7% at 5 A g^{-1} (2000 cycles)	[s20]
2.	MnO_2	N-rGO	93.2% at 5 A g^{-1} (7500 cycles)	[s21]
3.	$MnCo_2O_4$	N-rGO	85.2% at 1 A g^{-1} (3000 cycles)	[s22]
4.	$NiCo_2S_4$-3D Ni film@Ni wire	N-rGO	92% at 3 mA cm^{-2} (1000 cycles)	[s23]
5.	$Ni(OH)_2$/N-rGO	N-rGO	84.6% at 1 A g^{-1} (5000 cycles)	[s24]
6.	$NiCo_2S_4$-hallosyte	N-rGO	83.2% at 4 A g^{-1} (1700 cycles)	[s25]
7.	rGO/Ag/Ni_3S_2	N-rGO	82.5% at 4 A g^{-1} (8000 cycles)	[s26]
8.	Ni/$Ni(OH)_2$	N-rGO/FeO_X	91% at 9 A g^{-1} (10000 cycles)	[s27]
9.	rGO-CNT-Co_3S_4	N-rGO	90% at 5 A g^{-1} (3000 cycles)	[s28]
10.	N-doped rGO@ Bi_2O_3	N-rGO@$CoNi_2S_4$	85% at 10 A g^{-1} (10000 cycles)	[s29]
11.	NiCo LDH@N-doped graphene	N-rGO	82% at 2 A g^{-1} (2000 cycles)	[s30]
12.	$Co_3O_4/NiCo_2O_4$	N-rGO	93.8% at 12 mA cm^{-2} (10000 cycles)	**This work**

REFERENCES

[s1] Liu, S.; Xie, J.; Li, H.; Wang, Y.; Yang, H. Y.; Zhu, T.; Zhang, S.; Cao, G.; Zhao, X. Nitrogen-Doped Reduced Graphene Oxide for High-Performance Flexible All-Solid-State Microsupercapacitors. *J. Mater. Chem. A* **2014**, *2*, 18125–18131.

[s2] Gu, X.; Yang, Y.; Hu, Y.; Hu, M.; Huang, J.; Wang, C. Nitrogen-Doped Graphene Composites as Efficient Electrodes with Enhanced Capacitive Deionization Performance. *RSC Adv*. **2014**, *4*, 63189–63199.

[s3] Yan, L.; Punckt, C.; Aksay, I. A.; Mertin, W.; Bacher, G. Local Voltage Drop in a Single Functionalized Graphene Sheet Characterized by Kelvin Probe Force Microscopy. Nano Lett. **2011**, *11*, 3543–3549.

[s4] Yang, Y.; Shi, W.; Zhang, R.; Luan, C.; Zeng, Q.; Wang, C.; Li, S.; Huang, Z.; Liao, H.; Ji, X. Electrochemical Exfoliation of Graphite into Nitrogen-Doped Graphene in Glycine Solution and Its Energy Storage Properties. *Electrochim. Acta* **2016**, *204*, 100–107.

[s5] Li, S.-M.; Yang, S.-Y.; Wang, Y.-S.; Tsai, H.-P.; Tien, H.-W.; Hsiao, S.-T.; Liao, W.-H.; Chang, C.-L.; Ma, C.-C. M.; Hu, C.-C. N-Doped Structures and Surface Functional Groups of Reduced Graphene Oxide and Their Effect on the Electrochemical Performance of Supercapacitor with Organic Electrolyte. *J. Power Sources* **2015**, *278*, 218–229.

[s6] Jing, M.; Yang, Y.; Zhu, Y.; Hou, H.; Wu, Z.; Ji, X. An Asymmetric Ultracapacitors Utilizing α-$Co(OH)_2$/Co_3O_4 Flakes Assisted by Electrochemically Alternating Voltage. *Electrochim. Acta* **2014**, *141*, 234–240.

[s7] Huang, M.; Zhang, Y.; Li, F.; Zhang, L.; Wen, Z.; Liu, Q. Facile Synthesis of Hierarchical Co_3O_4@MnO_2 Core-Shell Arrays on Ni Foam for Asymmetric Supercapacitors. *J. Power Sources* **2014**, *252*, 98–106.

[s8] Wei, C.; Cheng, C.; Zhou, B.; Yuan, X.; Cui, T.; Wang, S.; Zheng, M.; Pang, H. Hierarchically Porous $NaCoPO_4$–Co_3O_4 Hollow Microspheres for Flexible Asymmetric Solid-State Supercapacitors. *Part. Part. Syst. Charact.* **2015**, *32*, 831–839.

[s9] Gao, Z.; Yang, W.; Wang, J.; Song, N.; Li, X. Flexible All-Solid-State Hierarchical $NiCo_2O_4$/Porous Graphene Paper Asymmetric Supercapacitors with an Exceptional Combination of Electrochemical Properties. *Nano Energy* **2015**, *13*, 306–317.

[s10] Shanmugavani, R.; Selvan, K. Microwave Assisted Reflux Synthesis of $NiCo_2O_4$/NiO Composite: Fabrication of High Performance Asymmetric Supercapacitor with Fe_2O_3. *Electrochim. Acta* **2016**, *189*, 283–294.

[s11] Niu, X.; Zhu, G.; Yin, Z.; Dai, Z.; Hou, X.; Shao, J.; Huang, W.; Zhang, Y.; Dong, X. Fiber-Based-All-Solid-State Asymmetric Supercapacitor Based on Co_3O_4@MnO_2 Core/Shell Nanowire Array. *J. Mater. Chem. A* **2017**, *5*, 22939–22944.

[s12] Pang, H.; Li, X.; Zhao, Q.; Xue, H.; Lai, W.-Y.; Hu, Z.; Huang, W. One-Pot Synthesis of Heterogeneous Co_3O_4-Nanocube/$Co(OH)_2$-Nanosheet Hybrid for High-Performance Flexible Asymmetric All-Solid-State Supercapacitors. *Nano Energy* **2017**, *35*, 138–145.

[s13] Xu, K.; Yang, J.; Hu, J. Synthesis of Hollow $NiCo_2O_4$ Nanospheres with Large Specific Surface area for Asymmetric Supercapacitors. *J. Colloid interface Sci*. **2018**, *511*, 456–462.

[s14] Wang, N.; Sun, B.; Zhao, P.; Yao, M.; Hu, W.; Komarneni, S. Electrodeposition Preparation of $NiCo_2O_4$ Mesoporous Film on Ultrafine Nickel Wire for Flexible Asymmetric Supercapacitors. *Chem. Eng. J.* **2018**, *345*, 31–38.

[s15] Wen, S.; Liu, Y.; Zhu, F.; Shao, R.; Xu, W. Hierarchical MOS_2 Nanowires/$NiCo_2O_4$ Nanosheets Supported on Ni Foam for High-Performance Asymmetric Supercapacitors. *Appl. Surf. Sci.* **2018**, *428*, 616–622.

[s16] Liu, Y.; Wen, S.; Shi, W. Co_3S_4 Nanoneedles Decorated on $NiCo_2O_4$ Nanosheets for High-Performance Asymmetric Supercapacitors. *Mater. Lett.* **2018**, *214*, 194–197.

[s17] Xing, L.; Dong, Y.; Hu, F.; Wu, X.; Umar, A. Co_3O_4 Nanowire@NiO Nanosheet Arrays for High Performance Asymmetric Supercapacitors. *Dalton Trans.* **2018**, *47*, 5687–5694.

[s18] Yin, Y.; Xu, Y.; Zhou, Y.; Yan, Y.; Zhan, K.; Yang, J.; Li, J.; Zhao, B. Milimeter-Long Vertically-Aligned Carbon Nanotube Supported Co3O4 Composite Electrode for High-Performance Asymmetric Supercapacitor. *ChemElectroChem* **2018**, *11*, 1394–1400.

[s19] Bhagwan, J.; Nagaraju, G.; Ramulu, B.; Sekhar, S. C.; Yu, J. S. Rapid Synthesis of Hexagonal $NiCo_2O_4$ Nanostructure for High-Performance Asymmetric Supercapacitors. *Electrochim. Acta* **2019**, *299*, 509–517.

[s20] Quan, H.; Cheng, B.; Chen, D.; Su, X.; Xiao, Y.; Lei, S. One-Pot Synthesis of α-MnS/Nitrogen-Doped Reduced Graphene Oxide Hybrid for High-Performance Asymmetric Supercapacitors. *Electrochim. Acta* **2016**, *210*, 557–566.

[s21] Iamprasertkun, P.; Krittayavathananon, A.; Seubsai, A.; Chanlek, N.; Kidkhunthod, P.; Sangthong, W.; Maensiri, S.; Yimnirun, R.; Nilmoung, S.; Pannopard, P.; Ittisanronnachai, S.; Kongpatpanicha, K.; Limtrakul, J.; Sawangphruk, M. Charge Storage Mechanisms of Manganese Oxide Nanosheets and N-doped Reduced Graphene Oxide Aerogel for High-Performance Asymmetric Supercapacitors. *Sci. Rep*. **2016**, *6*, 37560.

[s22] Pettong, T.; Iamprasertkun, P.; Krittayavathananon, A.; Suktha, P.; Sirisinudomkit, P.; Seubsai, A.; Chareonpanich, M.; Kongkachuichay, P.; Limtrakul, J.; Sawangphruk, M. High-Performance Asymmetric Supercapacitors of $MnCo_2O_4$ Nanofibers and N-Doped Reduced Graphene Oxide Aerogel. *ACS Appl. Mater. Interfaces* **2016**, *8*, 34045–34053.

[s23] Saravanakumar, B.; Jayaseelana, S. S.; Seo, M.-K. Kim, H.-Y.; Kim, B.-S. $NiCo_2S_4$ Nanosheet-Decorated 3D, Porous Ni Film@Ni Wire Electrode Materials for All-Solid-State Asymmetric Supercapacitor Applications. *Nanoscale* **2017**, *9*, 18819–18834.

[s24] Sirisinudomkit, P.; Iamprasertkun, P.; Krittayavathananon, A.; Pettong, T.; Peerapan, D.; Sawangphruk, M. Hybrid Energy Storage of $Ni(OH)_2$-Coated N-Doped Graphene Aerogel//N-Doped Graphene Aerogel for the Replacement of NiCd and NiMH Batteries. *Sci. Rep*. **2017**, *7*, 1124.

[s25] Chai, H.; Dong, H.; Wang, Y.; Xu, J.; Jia, D. Porous $NiCo_2S_4$-Halloysite Hybrid Self-Assembled from Nanosheets for High-Performance Asymmetric Supercapacitor Applications. *Appl. Surf. Sci*. **2017**, *401*, 399–407.

[s26] Qi, J.; Chang, Y.; Sui, Y.; He, Y.; Meng, Q.; Wei, F.; Ren, Y.; Jin, Y. Facile Synthesis of Ag-Decorated Ni_3S_2 Nanosheets with 3D Bush Structure Grown on rGO and Its Application as Positive Electrode Material in Asymmetric Supercapacitor. *Adv. Mater. Interfaces* **2018**, *8*, 1700985.

[s27] Liu, B.-T.; Zhao, M.; Han, L-P.; Lang, X.-Y.; Wen, Z.; Jiang, Q. Three-Dimensional Nanoporous N-Doped Graphene/Iron Oxides as Anode Materials for High-Density Energy Storage in Asymmetric Supercapacitors. *Chem. Eng. J*. **2018**, *335*, 467–474.

[s28] Mohammadi, A.; Arsalani, N.; Tabrizi, G. A.; Moosavifard, S. E.; Naqshbandi, Z.; Ghadimi, L. S. Engineering rGO-CNT Wrapped Co_3S_4 Nanocomposites for High-Performance Asymmetric Supercapacitors. *Chem. Eng. J*. **2018**, *334*, 66–80.

[s29] Zhao, J.; Li, Z.; Shen, T.; Yuan, X.; Qiu, G.; Jiang, Q.; Lin, Y.; Song, G.; Meng, A.; Li, Q. Oxygen-Vacancy Bi_2O_3 Nanosheets Arrays with Excellent Rate Capability and $CoNi_2S_4$ Nanoparticles Immobilized on N-Doped Graphene Nanotubes as Robust Electrode Materials for High-Energy Asymmetric Supercapacitors. *J. Mater. Chem. A* **2019**, *7*, 7918–7931.

[s30] Mehrabimatin, B.; Gilshteyn, E. P.; Buan, M. E. M.; Sorsa, O.; Jiang, H.; Zad, A. I.; Shahrokhian, S.; Nasibulin, A. G.; Kallio, T. Flexible and Mechanically Durable Asymmetric Supercapacitor based on NiCo Layered Double Hydroxide and Nitrogen-Doped Graphene Using a Simple Fabrication Method. *Energy Technol*. **2019**, *7*, 1801002.